Journal of Advanced Joining Processes 3 (2021) 100050

Contents lists available at ScienceDirect

Journal of Advanced Joining Processes

journal homepage: www.elsevier.com/locate/jajp

Exploitation of rubbery electrospun nanofibrous mat for fracture toughness improvement of structural epoxy adhesive bonded joints

S. Minosi[a,e,*], D. Cocchi[b], E. Maccaferri[c], A. Pirondi[a], A. Zucchelli[b], L. Mazzocchetti[c], D. Ambrosini[a,b], F. Campanini[d]

[a] Department of Engineering and Architecture, University of Parma, Parco Area delle Scienze 181/A, 43124 Parma, Italy
[b] Department of Industrial Engineering, Alma Mater Studiorum - University of Bologna, Viale del Risorgimento 2, 40136 Bologna, Italy
[c] Department of Industrial Chemistry "Toso Montanari", Alma Mater Studiorum - University of Bologna, Viale del Risorgimento 4, 40136 Bologna, Italy
[d] ELANTAS Europe Srl, Strada Antolini 1 loc. Lemignano, 43044 Collecchio, Parma, Italy
[e] Future Technology Lab, Parco Area delle Scienze 181/A, 43124 Parma, Italy

ARTICLE INFO

Keywords:
Bonded joints
Bonding reinforcement
Nanomaterials
Fracture toughness
Epoxy
Electrospinning

ABSTRACT

The improvement of the fracture toughness of adhesive joints is a key factor in many structural applications. The ability of nylon electrospun nanofibrous mat to act as an adhesive carrier and reinforcing web in adhesive bonding has been demonstrated by the Authors in previous works. It has been shown that the impregnation method developed and refined during the previous studies allow generating high-quality pre-preg nanomats out of a 2k unfilled epoxy resin. By applying this methodology, in the present work, rubbery nanofibrous mats have been adopted for the first time to reinforce and increase the fracture toughness of adhesive joints. Rubbery nanofibers were produced by electrospinning of nitrile butadiene rubber (NBR) and poly(ε-caprolactone) (PCL). The addition of the semi-crystalline polymer (PCL) is exploited to maintain the nanofibrous morphology, which the rubber alone (NBR) would not be able to ensure due to its low glass transition temperature (T_g). The nanofibers thus obtained have been integrated into a two-component high strength epoxy resin for structural applications. S235 steel adherends for Double Cantilever Beam (DCB) tests have been manufactured and sandblasted to improve adhesion. An optimization of the sandblasting parameters (distance, pressure, angle and time) has been carried out evaluating the shear strength and the fracture surfaces on S235 steel Single Lap Joints (SLJ). Finally, DCB tests have been performed to compare the mode I fracture toughness with and without the rubbery electrospun nanomats.

Introduction

Epoxy adhesives are widely adopted for structural bonded joints in several industrial fields, providing high strength combined with low weight (da Silva et al., 2011; Banea et al., 2018). Thanks to their highly cross-linked structure, epoxies show high elastic modulus and strength, good performance at high temperatures and reduced creep (Kinloch, 1987; Kinloch, 2005). However, their rigid structure also makes them extremely brittle and therefore barely resistant to crack initiation and propagation (Kinloch, 2003; Tsang and Taylor, 2019). To improve the strength of epoxy adhesive joints and thus avoid catastrophic failure, epoxy resins are commonly toughened by introducing fillers or modifying the chemical composition of the resin (Giv et al., 2018; Saraç et al., 2018). Thermally expandable particles (TEPs) also could be added to the adhesive to improve the fracture toughness of the system (Banea et al., 2014). Fracture toughness improvement by means of rubber addition is one of the most adopted methods to mitigate epoxy resin brittleness (Caldona et al., 2017). The rubber-toughening effect is commonly achieved either by adding already cross-linked (Riew et al., 1996; Williams et al., 1997) or core-shell rubbery particles (Tsang and Taylor, 2019) or by mixing the liquid rubber (i.e. not crosslinked) with resin precursors, thus forming rubbery particles due to the rubber precipitation during the resin cross-linking process (Williams et al., 1997; Wise et al., 2000). To improve the fracture toughness of epoxy systems, it has been shown that a rubber fraction between 5 and 20 %wt is required. Such a high amount, however, may negatively impact other mechanical and physical properties, reducing the glass transition temperature (T_g), the elastic modulus and the strength of the neat resin (Bagheri et al., 2009). Besides bulk rubber-like modifications, other ways to increase the fracture toughness of epoxies are the addition of different types of fillers, like particles or short fibers, both organic and inorganic (Kinloch, 2003; Giv et al., 2018). For instance, short glass

* Corresponding author at: Department of Engineering and Architecture, University of Parma, Parco Area delle Scienze 181/A, 43124 Parma, Italy.
E-mail address: stefania.minosi@unipr.it (S. Minosi).

https://doi.org/10.1016/j.jajp.2021.100050
Received 12 November 2020; Received in revised form 22 February 2021; Accepted 22 February 2021

Nomenclature

a	crack length
A	cross section of the adherent
b	width of the specimen
g	distance from load axis of CMOD measurement point
E	Young's modulus of the adherent
E_a	Young's modulus of the adhesive
E_{bend}	Flexural modulus of the adhesive
T_g	Glass transition temperature of the adhesive
G_I	Mode I strain energy release rate
G_{IC}	fracture toughness
h	thickness of the adherent
J	area moment of inertia of the adherent
k	elastic foundation stiffness (Krenk, 1992)
P	force
t	thickness of the bonding interface
δ'	Crack Mouth Opening Displacement (CMOD)
λ_σ	length scale of the stress distribution in a DCB joint (Krenk, 1992)
ν_a	Poisson's coefficient of the adhesive

fibers are broadly used as matrix reinforcement and toughening agent (Avci et al., 2004; Leonard et al., 2009). It was demonstrated that the use of nanoparticles leads to an effective increase in strength, stiffness and fracture toughness of epoxy adhesives joints (Giv et al., 2018). Engineered nanomaterials present useful properties such as high surface area and limited number of structural defects. Thermal, electrical, and mechanical properties of the polymeric matrix could be improved, depending on the quantity, size, nature, and interfacial adhesion of the integrated nanomaterials. A strong interfacial adhesion guarantees the correct load transfer from the polymeric matrix to the nano-reinforcement (Giv et al., 2018). Alumina nanospheres and nanorods integration shows both a significant increase of joint shear strength and mode I fracture toughness (Gupta et al., 2019). Similarly, carbon nanotubes (CNTs) and graphene nanoplatelets (GNPs) can be used as nano-reinforcements to improve stiffness, strength, fracture toughness and electrical conductivity of bonded joints (Takeda and Narita, 2017; Burkholder et al., 2011; Jakubinek et al., 2015; Gude et al., 2015; Korayem et al., 2016; Khoramishad and Khakzad, 2018; Akpinar et al., 2018; Zielecki et al., 2017; Jojibabu et al., 2019; Cha et al., 2019).

An efficient way to reinforce epoxy resins is the integration of polymeric nanofibers, even composite ones, inside the matrix (Huang et al., 2003). Many studies demonstrate that composite laminates reinforced with electrospun polymeric nanofibrous mats show improved mechanical properties (Zucchelli et al., 2011; Palazzetti and Zucchelli, 2017; Hamer et al., 2011). Polymeric thermoplastic nanomat interposition between composite layers activates a ply-to-ply bridging effect increasing both mode I and mode II fracture toughness and fatigue delamination strength (Palazzetti et al., 2013; Moroni et al., 2013; Giuliese et al., 2015; Beckermann and Pickering, 2015; Saghafi et al., 2015; Zhang et al., 2015; Daelemans et al., 2016; Daelemans et al., 2017). These results suggest a possible application of such nanomats for promoting crack toughening of bonded joints. Currently, only a few papers explore the use of electrospun nanofibers in adhesives bonding (Oh et al., 2014; On et al., 2017; Razavi et al., 2018; Ekrem and Avcı, 2018). In (Razavi et al., 2018) Double Cantilever Beam (DCB) joints were produced from aluminium substrates, bonded with 2k epoxy resin on which polyacrylonitrile (PAN) nanofibers were directly electrospun. DCB tests show up to a two-fold increase in fracture toughness compared to neat epoxy resin, although the baseline value was quite low (G_C = 0.11 N/mm over 30 mm of crack propagation). In (Ekrem and Avcı, 2018) poly(vinyl alcohol) (PVA) nanofibrous mats were placed inside the adhesive layer of Single Lap Joints (SLJ) and DCB joints: shear strength increased by 13.5%, while mode I fracture toughness was about twice the neat adhesive. The ability of nylon 66 electrospun nanofibrous mat to act as adhesive support and reinforcing web in adhesive bonding has been demonstrated in previous works by the Authors (Musiari et al., 2018; Brugo et al., 2018; Cocchi et al., 2020). The impregnation method developed and refined during the previous studies allows generating high-quality pre-preg nanomats out of a 2k unfilled epoxy resin. This allows using the nanomat directly as a pre-preg carrier for the uncured adhesive instead of traditional glass fiber carrier, promoting at the same time crack toughening of the bonded joint.

Recently, the possibility of producing uncross-linked rubbery nanofibers was demonstrated (Maccaferri et al., 2020), as well as their excellent ability to hinder delamination in epoxy CFPR laminates by increasing significantly the mode I interlaminar fracture toughness (Maccaferri et al., 2020). It was also found an enhancement of the CFRP damping, thanks to the toughening action of this type of nanofibers.

In the present work, Nitrile Butadiene Rubber / poly(ε-caprolactone) (NBR/PCL) rubbery nanofibrous mats have been adopted for the first time to reinforce epoxy adhesive joints with the aim at increasing its fracture toughness. By applying the same methodology as in (Musiari et al., 2018; Brugo et al., 2018; Cocchi et al., 2020), an attempt was made to combine the well-known rubber-toughening action with the ease of integration of electrospun nanofibrous pre-pregs inside bonded joints. The use of rubbery nanofibers, besides potentially improving fracture toughness, it also could enhance the damping properties of the adhesive joint, without significantly compromising its mechanical performance and weight. S235 steel adherents for Double Cantilever Beam (DCB) tests have been manufactured and sandblasted to improve adhesion. An optimization of the sandblasting parameters (distance, pressure, angle and time) has been carried out for evaluating the shear strength and the fracture surfaces on S235 steel Single Lap Joints (SLJ). Finally, DCB tests have been performed to compare the mode I fracture toughness with and without the rubbery electrospun nanomats. The correct determination of the mode I fracture toughness is crucial for evaluating the rubbery nanomat integration effect and curing cycle influence. Several data reduction methods exist to overcome the difficulty in the direct monitoring of the crack length during the DCB test. Data reduction schemes include the compliance calibration method, which calibrates the compliance as a polynomial function of crack length, and the compliance-based beam method, which takes into account the influence of the fracture process zone (Han et al., 2020; Yan et al., 2020; Fernández et al., 2011). In this paper a beam theory-based model was used that considers the elastic behaviour of the adhesive bondline by modelling the DCB joint as a beam on an elastic foundation.

Experimental methodology

NBR/PCL nanofibrous mat

The production of Nitrile Butadiene Rubber / poly(ε-caprolactone) (NBR/PCL) rubbery nanomat followed the methodology reported in (Maccaferri et al., 2020). The innovative approach adopted allows to electrospin NBR-based nanofibers without the need of a crosslinking step of the rubber, since the obtained blend nanofibers mimic the behaviour of a thermoplastic elastomer (TPE).

Carboxylated NBR (NIPOL 1072CGX) was supplied from Zeon Chemicals (Lousville, USA), while PCL was purchased from Sigma-Aldrich (Milan, Italy). Both polymers were used without any preliminary treat-

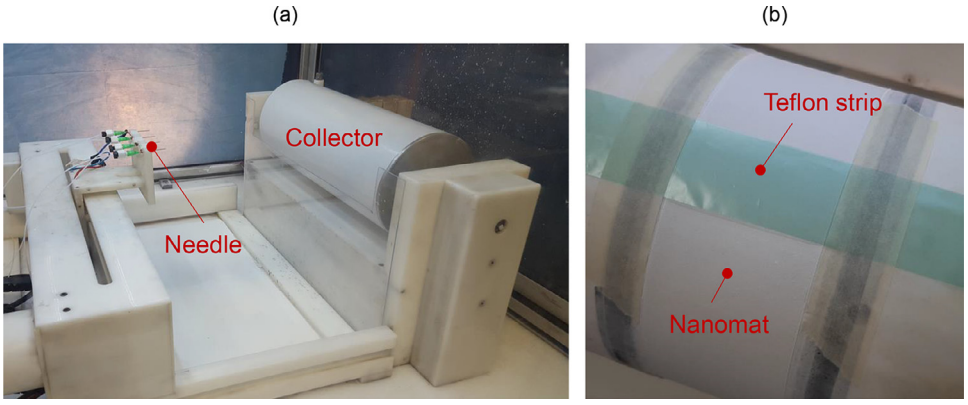

Fig. 1. Electrospinning machine setup (a) and PTFE strip placement to produce the initial defect (b).

Table 1
Electrospinning parameters for N-60/40 nanomat production.

Electrospinning parameters	
Flow rate	0.55 mL/h
Electric potential	18.3 kV
Distance	13 cm
Electric field	1.4 kV/cm
Temperature	22–26 °C
Relative Humidity (RH)	23–25%

ment. N,N-dimethylacetamide (DMAc), N,N-dimethylformamide (DMF) and chloroform ($CHCl_3$) for solutions preparation were purchased from Sigma-Aldrich and used without further purifications. PCL is a semi-crystalline polymer characterized by a glass transition temperature (T_g) at −58 °C and by a melting temperature (T_m) near 60 °C, while the NBR, being amorphous, does not show melting (it is characterized by two T_gs centered at −14 and −42 °C).

A solution containing 10 %wt of NBR was prepared in DMAc under magnetic stirring at room temperature until the formation of a homogeneous solution, named S-NBR. Similarly, a 10%wt PCL solution was prepared in DMF/$CHCl_3$ 1:1wt solvent system, under magnetic stirring at room temperature until the formation of a homogeneous solution, named S-PCL. The NBR/PCL blend was prepared by mixing S-NBR and S-PCL in a 60:40 weight ratio to obtain NBR/PCL blend nanofibers with a 60 %wt of NBR content, named N-60/40. The electrospinning machine used was equipped with one 5 mL syringe jointed to the needle (internal diameter 0.84 mm, 55 mm length) via a Teflon pipe. A grounded drum collector, shown in Fig. 1a, was used to collect the nanofibers (tangential speed 0.40 m/s). The process and environment parameters used are summarized in Table 1.

Two 50 mm width strips were electrospun in order to obtain the patches necessary for the DCB joints production. The initial defect was created during the nanomat production. To this end, after the electrospinning of the first half-thickness of the nanomat, a PTFE strip of the desired length was placed on the nanofibrous mat to produce the initial defect, as shown in Fig. 1b. Then, the second half-thickness of the nanomat was electrospun. Before integration into the epoxy resin, the patches for DCB joints were cut to the final size of 150 × 25 mm^2.

The thickness of the nanomat is in the 80–110 μm range. This value was measured along the nanomat strip by a digital indicator (ALPA Megarod, Pontoglio (BS), Italy) with a measuring pressure of 100 g/cm^2. N-60/40 nanofibrous mat morphology was analysed by scanning electron microscopy (SEM, Phenom ProX, ThermoFisher Scientific, Waltham, USA). Fig. 2 shows SEM images of N-60/40 nanomat at different magnifications. The fibers diameter is 268 ± 62 nm. Average values derived from manual measurement of >100 single fiber diameters using the Photoshop measurement tool.

Adhesive

A structural 2k epoxy resin supplied by ELANTAS Europe SRL (Collecchio (PR), Italy) was used to manufacture DCB joints. The epoxy system, named Elan-tech® AS90/AW91, was depleted from thixotropic agents by the supplier in order to reduce the resin viscosity and to improve the wettability of the nanofibers without affecting mechanical properties. The resin was supplied in cartridges to limit the possible air entrapment via manual mixing. Adhesive bulk properties from Elan-tech® AS90/AW91 technical datasheet are detailed in Table 2.

Adherents

A cold drawn S235 steel bar was cut and machined to obtain 150 × 25 × 10 mm^3 DCB adherents. The metal supports were used to realise DCB joints with “virgin” adhesive, named “V”, and nano-reinforced one, named “N”, with rubbery nanofibrous mat integrated into the adhesive layer. The elastic modulus of the steel is assumed to be 210 GPa, while its yield strength being 235 MPa. On each adherent, one perforated steel block, is bonded to connect the specimen to the testing machine was bonded. The geometry of the DCB adherents is reported in Fig. 3. The steel adherent dimensions were reduced if compared with ASTM D3433 standards. This non-standard size has been selected to simplify the manipulation of the nanomat, after the impregnation with epoxy resin. The steel surfaces were degreased with acetone, sandblasted and then sonicated for 60 s in acetone. Sandblasting is the simplest and most effective method to increase the surface roughness of the substrate to bond (Ebnesajjad and Ebnesajjad, 2014; Kozma and Olefjord, 1987; da Silva et al., 2009; Wegman, 1989; van Dam et al., 2020).

In fact, roughness influences chemical bonds and mechanical interlocking between adhesive and adherents. Increasing the roughness also increases the contact area between adhesive and substrate and, therefore, chemical and mechanical interaction improve. The parameters that most influence the sandblasting process have been identified in the literature (Poorna Chander et al., 2009; Amada and Satoh, 2000; Fernando et al., 2013), that are distance of blasting gun nozzle from the substrate, blasting time, pressure and angle. For each parameter, two values were considered, as reported in Table 3.

A series of SLJs have been manufactured and tested to identify the best set of sandblasting parameters for the treatment of S235 bonding surfaces. Sandblasting parameters optimization was performed by SLJ for ease of execution. DCB tests, in fact, require more time compared to SLJ ones due to the pre-cracking phase. Although loading mode differs from DCBs, SLJs represent a valid tool to evaluate surface treatment effectiveness and epoxy adhesion on the sandblasted steel supports. The adhesive used for SLJ is the same of DCB joints. The joints standard cure cycle suggested by the supplier is to keep it at 70 °C for 5 h. For each combination of the sandblasting parameters, three SLJ were manufactured and tested according to ASTM D1002 standard. The final values

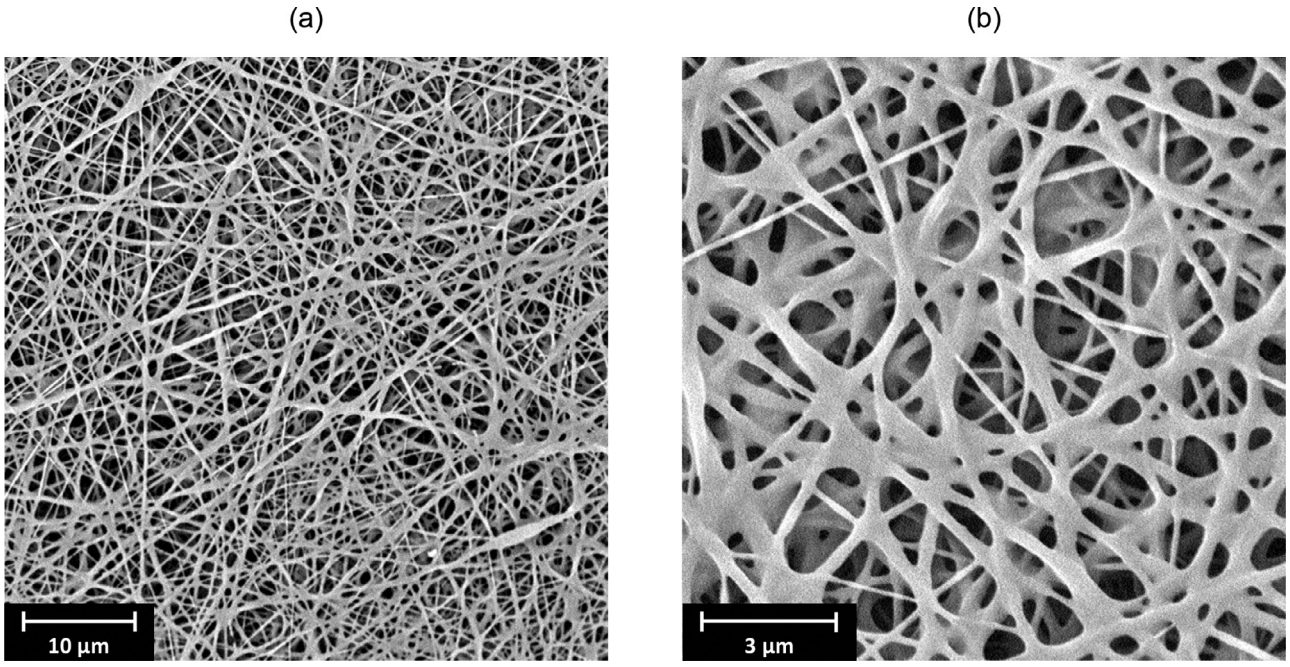

Fig. 2. SEM images of NBR/PCL nanofibrous mat N-60/40 at 5,000x (a) and 20,000x (b).

Table 2
Bulk properties at room temperature of the two-part epoxy adhesives Elan-tech® AS90/AW91, (ELANTAS Europe srl, Italy).

Property	Units	Value
Viscosity	mPa•s	5000
Gel Time	h	5–6
Cure cycle suggested by the supplier	h	5
	°C	70
Glass transition temperature (ASTM D3418) after 24 h at RT	°C	40–47
Flexural strength (ASTM D790)	MPa	70–80
Strain at break (ASTM D790)	%	4.5–7.5
Flexural modulus (ASTM D790)	MPa	2000–2500
Tensile strength (ASTM D638)	MPa	45–55
Elongation at break (ASTM D638)	%	4.5–6.5
Shear strength (ASTM D1002) on AISI 316, cured 5 h at 70 °C	MPa	24.5–29.5
Peel strength (ASTM D1876) on Aluminum, cured 5 h at 70 °C	N/cm	35–43

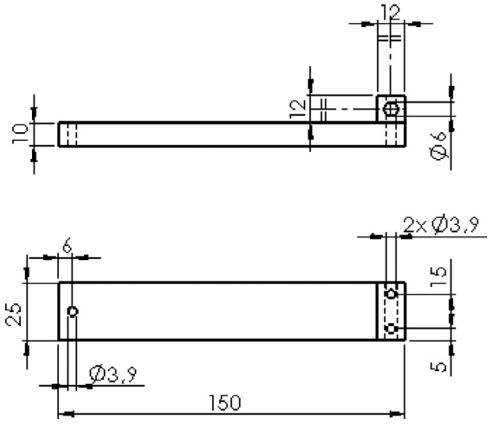

Fig. 3. DCB adherent geometry.

Table 3
Sandblasting parameters.

Sandblasting parameters	Values	
Distance (cm)	8	13
Pressure (bar)	2	6
Angle (deg)	75	90
Time (s)	10	60

of sandblasting parameters were selected after the evaluation of surface roughness, the average shear strength and type of fracture of SLJ.

From the analysis of the SLJs test results, the combination selected for DCB sandblasting, showed a cohesive type of fracture and has higher average shear strength values than the other samples, as well as a low standard deviation. The combination consists of a pressure of 6 bar, a nozzle distance of 8 cm, a nozzle angle of 90 °C with respect to the sample surface and an overall sandblasting time of 10 s for the SLJ. With these parameters, the surface roughness value is about 3.86 ± 0.06 µm. In Fig. 4 it is shown a SLJ sandblasted with parameters of the selected configuration. In this case the type of fracture is clearly cohesive.

DCB fabrication

Two classes of DCB joints, which differ for the applied curing cycle, were produced to evaluate the fracture toughness of the adhesive system with and without the integration of a rubbery nanomat. The first type

Fig. 4. SLJ exhibiting a cohesive type of fracture.

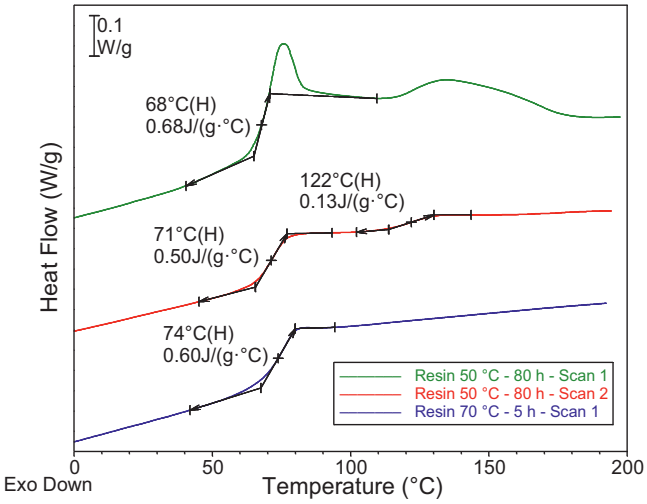

Fig. 5. DSC analysis of neat adhesive V 50 cured at 50 °C for 80 h and V 70 cured at 70 °C for 5 h.

of curing cycle is the standard one (cycle A, 70 °C for 5 h) with slow heating and cooling phases.

The second curing cycle was defined to account for nanofibers thermal stability since their structure is characterized by the presence of a crystalline phase of PCL that melts in the temperature range between 55 and 65 °C (Maccaferri et al., 2020). For this reason, temperatures above 65 °C cause the nano-fiber melting and the dispersion of both polymeric components within the matrix while the nanofibrous structure can be preserved by applying curing temperatures below the PCL melting. Consequently, cycle B consists of a temperature of 50 °C for 80 h to maintain the nanofibers structure. The flexural modulus (E_{bend}) of the neat resin was evaluated with a three-point bending test, for both curing cycles, according to the ASTM D790 standards. The epoxy resin cured with cycle A shows E_{bend} equal to 2447 ± 30 MPa, while the adhesive cured with cycle B shows a slightly lower E_{bend} (2330 ± 23 MPa). A DSC analysis of V 50 shows that even this low-T curing cycle leads to a significantly high cross-linking of the epoxy system, as proved by the attained T_g around 70° C, that goes almost unchanged upon reheating (Fig. 5). Moreover, the V 50 T_g is just slightly lower than the higher-T cured V 70, that during the first heating already reaches a glass transition above 70 °C.

The addition of the nanofibers to the resin leads to some peculiar behaviour. While, indeed, the curing temperatures were selected in order to either avoid or promote the melting of thermoplastic PCL component, Fig. 6, reporting the comparison of the DSC scans of N 50 and N 70, reveals in both cases the presence of an endothermic peak positioned in the region typical for nanofiber melting (Maccaferri et al., 2020): such a peak is expected, and indeed detected for N 50, while it is unexpected in N 70. The explanation for such a behaviour can be found in the signal that follows the endotherm, a stepwise transition that accounts for the glass transition of the resin reached during curing. It can be observed that in both cases the melting of PCL occurs when the resin is still in an almost glassy state, and this is the reason while PCL was not able to blend with neighbouring epoxy matrix even when brought above its melting. On the other side, increasing the curing temperature seems to promote the blending of the highly mobile rubbery phase: N 70 displays, indeed, a lower T_g due to a higher extent of rubber blending with neighbouring epoxy matrix. A similar behaviour is not observed in N 50 where the diffusion of the NBR out of the nanofibers is hampered by the lack of PCL melting and, as a consequence, the resin does not undergo plasticization, keeping a T_g similar to the plain VV 50 sample. It is worth to point out that due to the signal overlapping it was not possible to correctly determine the T_gs of the nano-modified samples. Summarizing, DSC tests suggest that both the applied curing temperatures are not able to promote full PCL miscibility with the epoxy resin, resulting in phase separated PCL fraction within the epoxy matrix after curing.

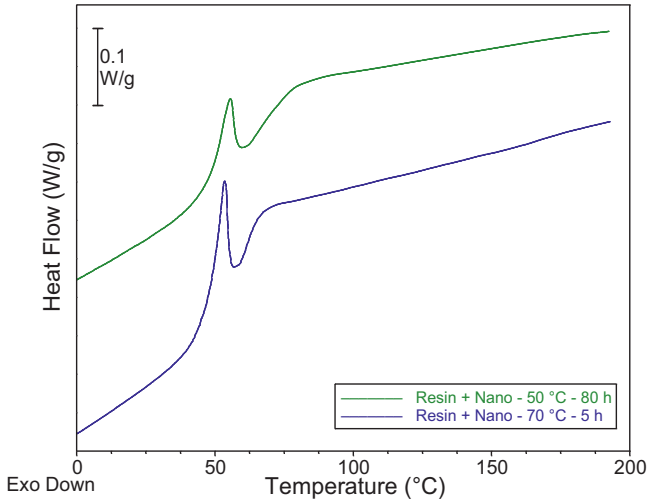

Fig. 6. DSC analysis of nanofiber modified adhesive N 50 cured at 50 °C for 80 h and N 70 cured at 70 °C for 5 h.

Table 4
DCB specimens series.

Series name	Adhesive layer	Curing cycle	Number of specimens
V 70	AS90/AW91	A - 70 °C for 5 h	3
V 50	AS90/AW91	B - 50 °C for 80 h	3
N 70	AS90/AW91 + N-60/40	A - 70 °C for 5 h	3
N 50	AS90/AW91 + N-60/40	B - 50 °C for 80 h	3

The four series of specimens produced are describes in Table 4.

The steel bonded surfaces were sandblasted, as previously defined. Each adherent was sonicated in acetone for 60 s before bonding. The nano-reinforced joints of the series N 70 and N 50 were manufactured by placing the nanomat prepreg between the two adherents. The prepreg was produced according to the laboratory route developed in previous works (Musiari et al., 2018; Brugo et al., 2018; Cocchi et al., 2020), that ensured the good impregnation of a nylon electrospun nanomat. The rubbery nanomat impregnation process begins by positioning a nanomat strip on a layer of epoxy resin spread on a Teflon-cover plate, then an

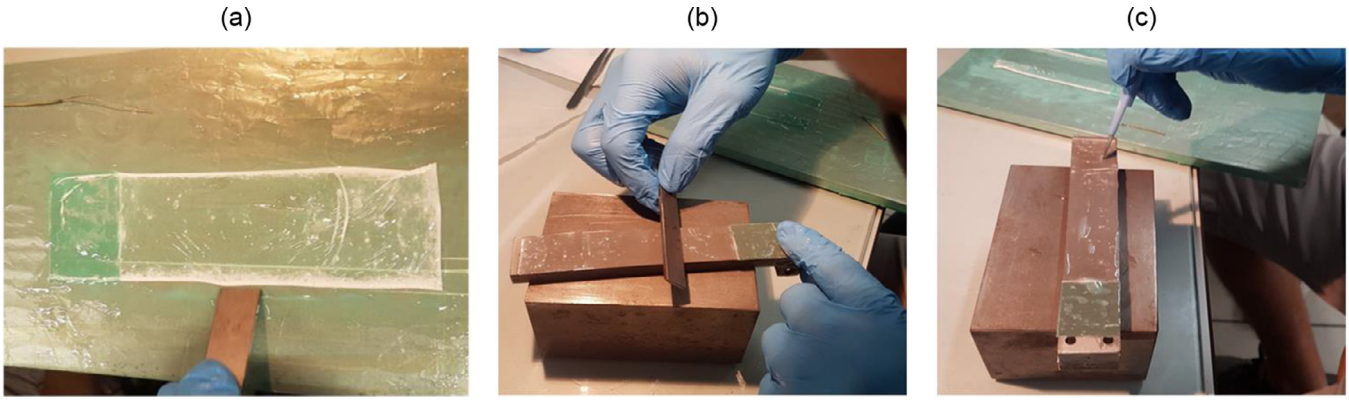

Fig. 7. Nano-reinforced DCB production process images: (a) nanomat impregnation, (b) nanomat placemen on sandblasted adherents and (c) air bubble removal with a needle.

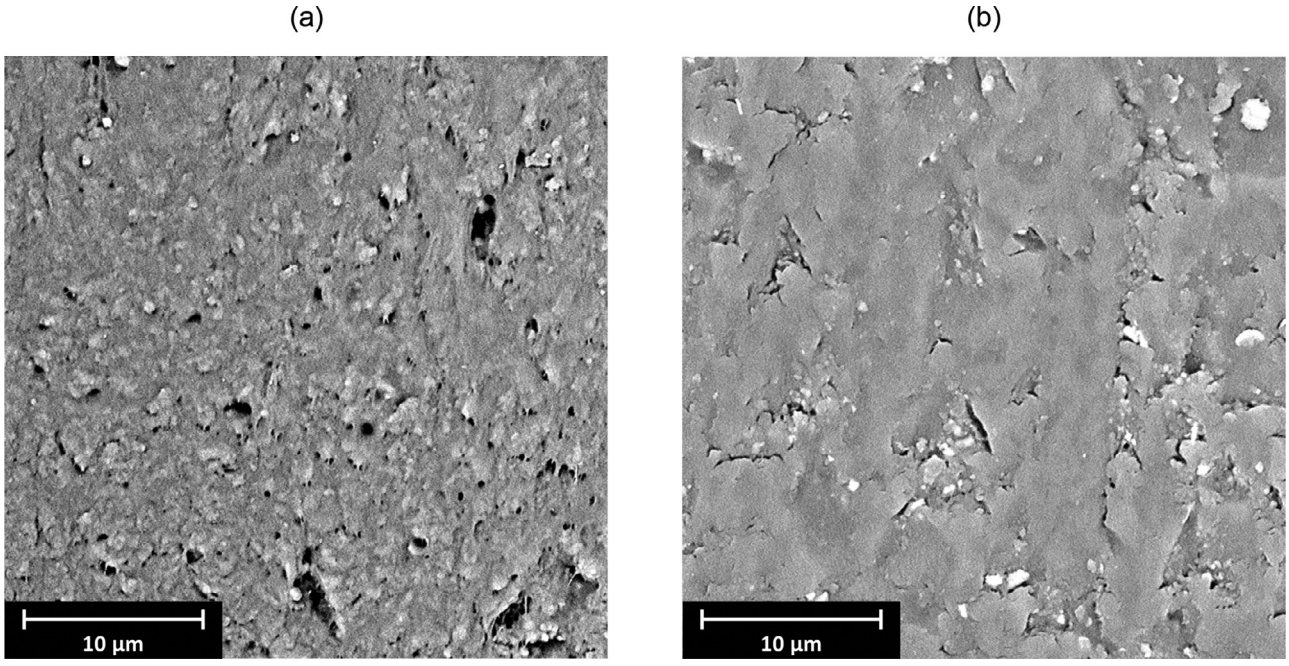

Fig. 8. Cross-sections of the joints cured at 70 °C for 5 h (a, cycle A) and at 50 °C for 80 h (b, cycle B).

additional amount of resin is deposited on the nanomat strip to favour its impregnation, as shown in Fig. 7a. When the nanomat is fully impregnated, the resin excess is removed with a spatula.

The effectiveness of the impregnation has been assessed through SEM analyses on additional nano-reinforced S235 steel joints subjected to the curing cycles previously defined as A and B. Fig. 8 shows cross-sections of the joints cured at 70 °C for 5 h (Fig. 8a, cycle A) and at 50 °C for 80 h (Fig. 8b, cycle B).

The SEM images reveal that the curing cycle A causes the NBR/PCL blend mixing with the epoxy resin, leading to toughened matrix. Respect to the curing cycle B, the fracture surfaces appear more irregular with pronounced indented markings. Instead, the nano-modified adhesive cured at low-T (cycle B) shows surfaces more brittle and regular, due to the lower toughening caused by the limited spread of the rubbery component from the nanofibers.

The prepreg obtained with the aforementioned procedure, already pre-cracked with a 30 mm long defect (see the section on nanomat production) is then positioned on the sandblasted surface of one metal adherent, as represented in Fig. 7b. Possible air bubbles inside the prepreg are removed with a needle, as shown in Fig. 7c. In general, this laboratory route ensures that the nanofibers are uniformly distributed into the bondline and there are no massive amounts of air bubbles inside the nano-reinforced matrix. The second adherent was overlapped and bolted together with the first one at the joint extremities.

The virgin DCBs of the series V 70 and V 50 were realized by placing metal spacers at the ends of one adherent of the junction. The spacers are 100 µm thick to obtain the same thickness as the nano-reinforced joints. A 30 mm long defect was introduced by placing a PTFE strip on the same adherent. The adherents, then, were overlapped and closed together with bolts and nuts at the joint extremities. The DCB whole geometry is reported in Fig. 9. Each series of DCBs was then subjected to the corresponding curing cycle. The bolts and nuts were removed after the polymerization.

DCB testing

The joints, represented in Fig. 9, were tested under displacement control at a constant crosshead velocity on a servo-hydraulic MTS 810 testing machine equipped with a 3 kN load cell. The Crack Mouth Open-

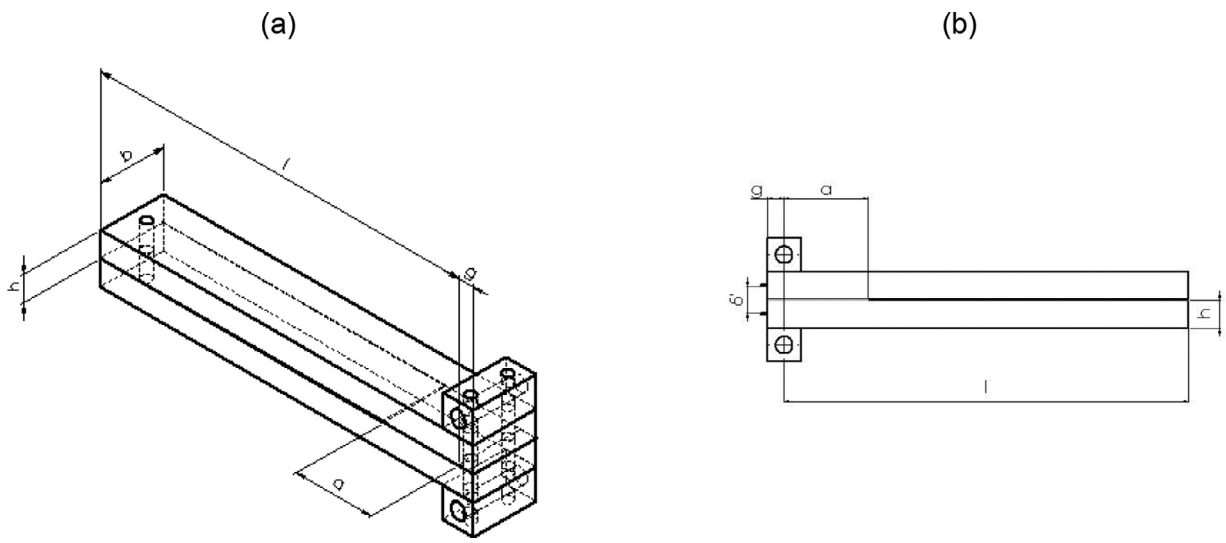

Fig. 9. DCB structure scheme: (a) 3-dimensional view and (b) side view.

ing Displacement (CMOD), δ', is evaluated by a clip gage. Fatigue pre-cracking was done at 5 Hz under load control until the crack has propagated 5 mm. The tests have been performed with partial un-loadings to evaluate the specimen compliance and therefore the actual crack length, calculated through the model reported in (Krenk, 1992). Each adherent is modelled as a beam on an elastic foundation and considers the out of plane deformation of the adhesive layer and the rotation at the crack tip. The model, represented by Eq. (1), has been modified to take into account the distance g of the CMOD measurement point from the load axis (g in Eq. 1) and the effect of shear (term on right in Eq. (1)).

$$\frac{\delta'}{P} = 2\left[\frac{2\lambda_\sigma}{k}\left(1+\lambda_\sigma a\right) + (a+g)\frac{\left(2\lambda_\sigma^2\right)}{k}\left(1+2\lambda_\sigma a\right) + \frac{a^3}{3EJ} + g\frac{a^2}{2EJ}\right] \quad (1)$$

The parameters λ_σ and k are reported in Eqs. (2) and (3):

$$\lambda_\sigma = 4\sqrt{\frac{6}{h^3 t}\frac{E_a}{E\left(1-v_a^2\right)}} \quad (2)$$

$$k = \frac{2E_a b}{t\left(1-v_a^2\right)} \quad (3)$$

The strain energy release rate G is:

$$G = \frac{(Pa)^2}{bEJ}\left(1+\frac{1}{\lambda_\sigma a}\right)^2 \quad (4)$$

The adhesive Young's modulus, E_a, was considered equal to the experimental flexural modulus evaluated by 3PB tests (E_{bend}) and $\nu_a = 0.4$ as common in epoxies. Since the fiber volume fraction negligible, for the rule of mixtures, also the Young's modulus of the nanomat pre-preg is approximately the same of the adhesive alone.

Results

The graphs in Fig. 10 report the load P against the CMOD, δ', of a representative sample for both virgin and nano-reinforced specimens. In particular in Fig. 10a, the results of joints named V 70 - 2 and N 70 - 3 cured at 70 °C for 5 h are reported, while Fig. 10b shows the results of joints V 50 - 3 and N 50 - 1, both cured at 50 °C for 80 h. Fig. 11 shows the R-curves of each specimen, specifically Fig. 11a refers to V 70 and N 70 series, while Fig. 11b refers to V 50 and N 50 series. For an easier visualization, in Figs. 10 and 11 the solid curves represent the virgin specimens of V 70 and V 50 series, while the dashed ones refer to the nano-reinforced specimens of the N 70 and N 50 series. In Fig. 11, the black markers identify the G_{IC} values considered for the calculation of the average fracture toughness during the steady-state crack propagation phase (i.e. after the load peak), while the grey markers represent instead the values excluded from the calculation. The results obtained for each samples series are summarized in Table 5 that reports the type of fracture surfaces and the average values of fracture toughness G_{IC}.

Table 5
DCB test result related to the type of fracture, the G_{IC} average value and the standard deviation.

	Type of fracture	G_{IC} (N/mm)	StandardDeviation (N/mm)
V 70	Cohesive	1,05	0,28
N 70	Cohesive	0,63	0,12
V 50	Adhesive	0,22	0,07
N 50	Cohesive	0,58	0,07

The analysis of the results reveals that the V 70 specimens, cured at 70 °C for 5 h, exhibit the highest values of G_{IC}, about 1,05 N/mm and cohesive fracture surfaces, as is shown in Fig. 12a. On the contrary, the V 50 joints, cured at lower temperature for a longer time, present a weak adhesion to the sandblasted steel adherends, resulting in adhesive fracture, as shown in Fig. 12c, and low values of G_{IC}, about 0.22 N/mm. From the SEM images in Fig. 13a is clear that the fracture surfaces of the V 70 - 2 sample is characterized by the presence of micro-dimples into the adhesive layer, which proves that ductile fracture mechanisms occurred in the neat resin and justifies the higher fracture toughness values. The fracture surface of the sample V 50 - 3 (Fig. 13b) exhibits moderate roughness and no micro-dimples, as the adhesive was not deformed in a ductile way. Since it was demonstrated that curing at 50 °C for 80 h provides a complete resin crosslinking (see Fig. 5), the poor adhesion may be related to a different time-viscosity (wettability) profile of the adhesive under these conditions. Therefore, beside an assessment of the time-viscosity profile at 50 °C and a comparison with that at the standard curing temperature of 70 °C, a dedicated surface treatment might be necessary under non-standard curing conditions. The R-curve behaviour of virgin DCBs cured at 70 °C is more scattered than the nano-reinforced ones that show an increasing trend for all the N specimens. The V 50 specimens also exhibit an increasing trend of R-curves, particularly after the Δa range $40 \div 50$ mm.

Nano-reinforced joints exhibit the same fracture toughness value ($G_{IC} = 0.63 \pm 0.12$ N/mm for N 70 and $G_{IC} = 0.58 \pm 0.07$ N/mm for N 50) and similar failure mechanisms independently from the curing cycle

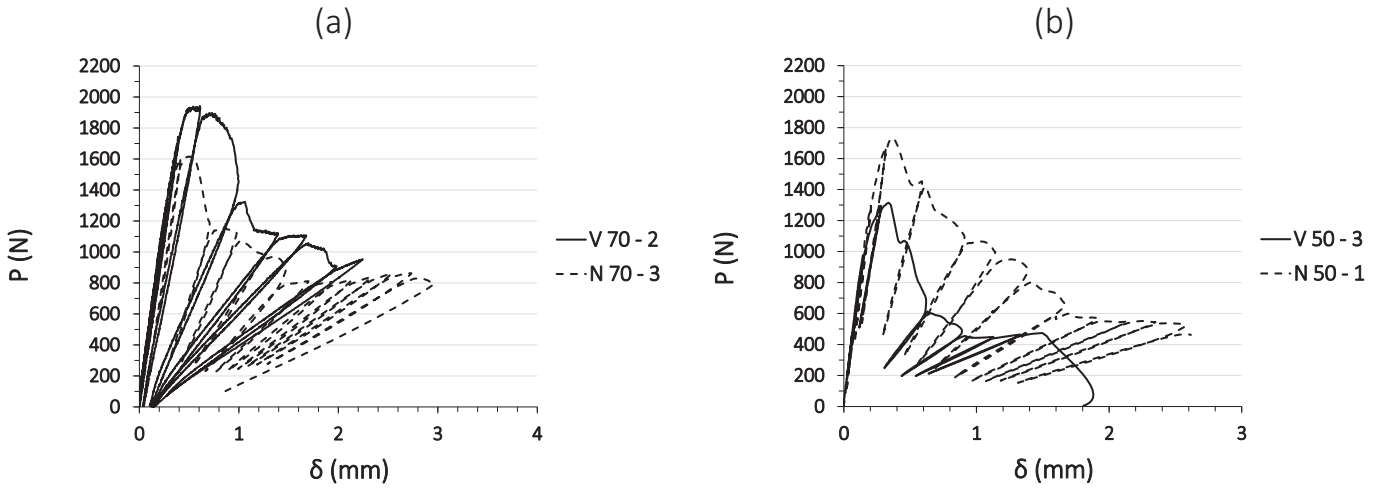

Fig. 10. Load against CMOD (δ') for both a virgin and nano-reinforced specimens cured at 70 °C for 5 h (a, cycle A) and at 50 °C for 80 h (b, cycle B), taken as representative. Solid lines refer to virgin specimens, while dashed lines refer to nano-reinforced ones.

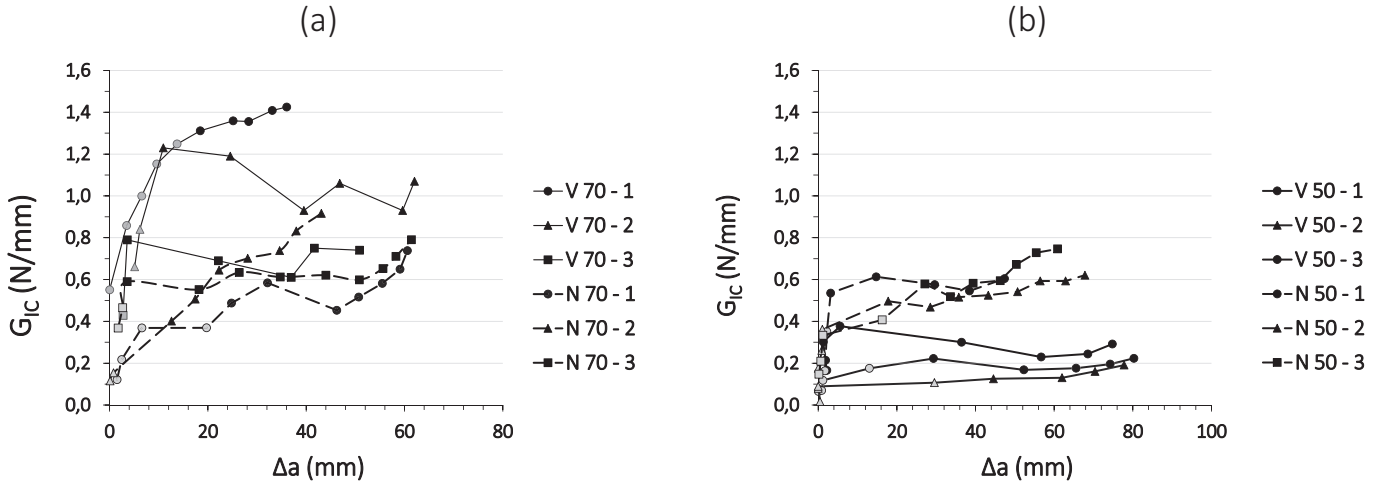

Fig. 11. R-curves for specimens cured at 70 °C for 5 h (a, cycle A) and at 50 °C for 80 h (b, cycle B). Solid lines refer to virgin specimens, while dashed lines refer to nano-reinforced ones. The black markers of the R-curves graph indicate the G_{IC} values considered for the steady-state fracture toughness average value calculation, whilst the grey ones the excluded values.

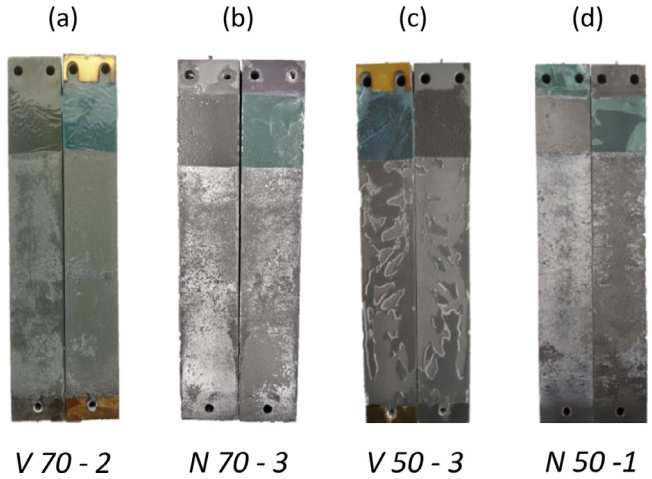

Fig. 12. Fracture surface after DCB test on V 70 - 2 (a), N 70 - 3 (b), V 50 - 3 (c) and N 50 - 1 (d).

used. Fig. 12b shows that the fracture surface of N 70 - 3 is cohesive, similarly to the nonreinforced joints cured at 50 °C, as reported in Fig. 12d. The SEM images of the nano-reinforced specimens, N 70 - 1 (Fig. 14) and N 50 – 1 (Fig. 15), show comparable and quite rough fracture surfaces. Fig. 14c represents a detail of the rubbery nanofibers that still partially maintain their structure due to the impossibility to complete PCL melting during curing cycle, even if performed at 70 °C. Indeed, while at 70 °C PCL is able to melt, this phenomenon probably occurs after the gel point of the adhesive during curing, hindering thermoplastic mixing with the epoxy resin. The samples cured at 50 °C for 80 h completely preserved their nanofibrous structure (Fig. 15c). However, the average fracture toughness of the adhesive is negatively affected by the nanomat integration. The G_{IC} value is reduced by 40% compared with the V 70 joints. On the other hand, the nanofiber integration enables the cracks propagation within the adhesive layer, even at 50 °C, because the nanofibrous structure retains the resin that does not flow away during the first stage of the crosslinking process. In this way, the presence of the nanomat ensures good adhesion between the adhesive layer and the steel support and the risk reduction of uncontrollable adhesive fractures.

Although the integration of the nanomat reduces the overall fracture toughness of the adhesive joint, it is interesting to note that nano-reinforced joints show a constant fracture toughness trend as the crack propagates (see Fig. 11, R-curves). It seems that nanofibers allow for a more reproducible result, regardless of the curing cycle adopted. Although performance may be reduced, a guaranteed minimum G_{IC} fracture toughness value seems to be achieved.

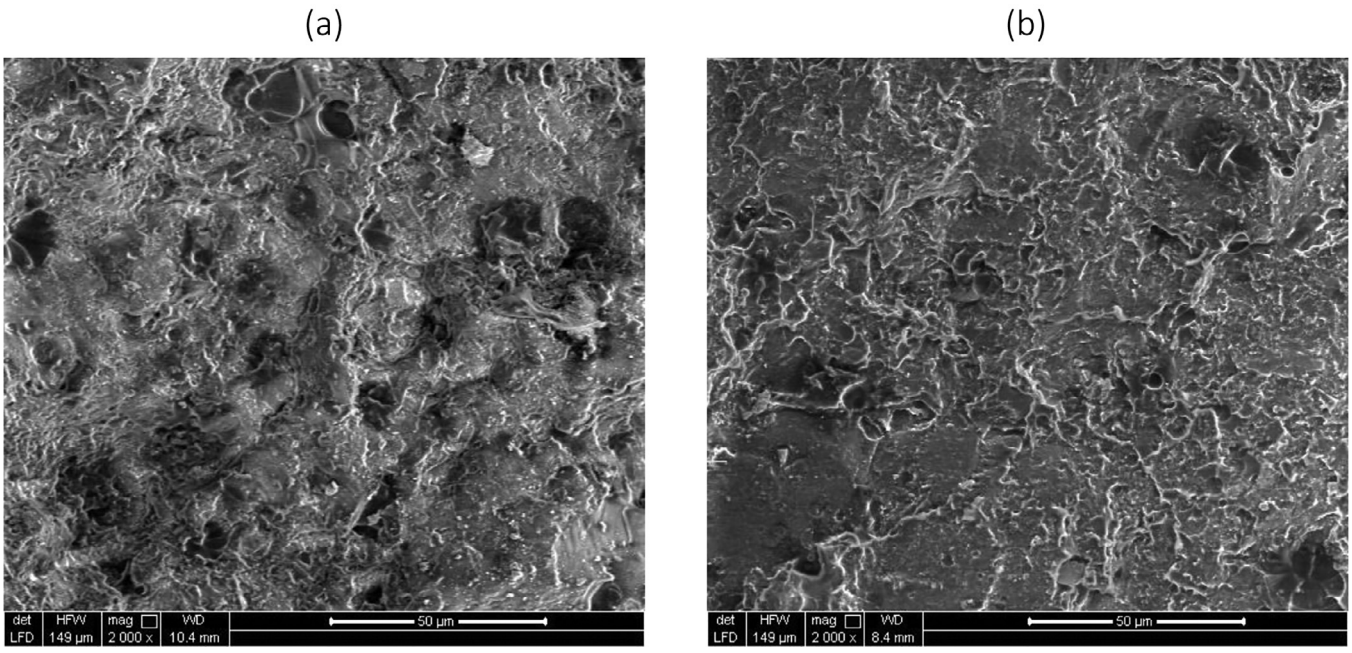

Fig. 13. SEM images of fracture surfaces of (a) V 70 - 2, (b) V 50 - 3 samples.

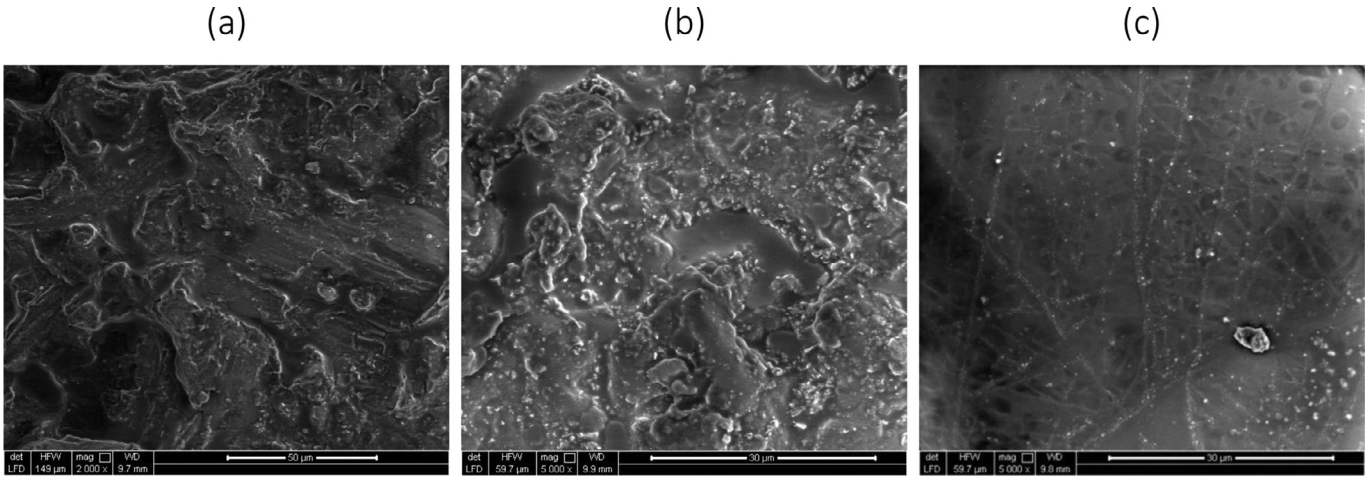

Fig. 14. SEM images of fracture surfaces of N 70 - 1 sample at different magnifications.

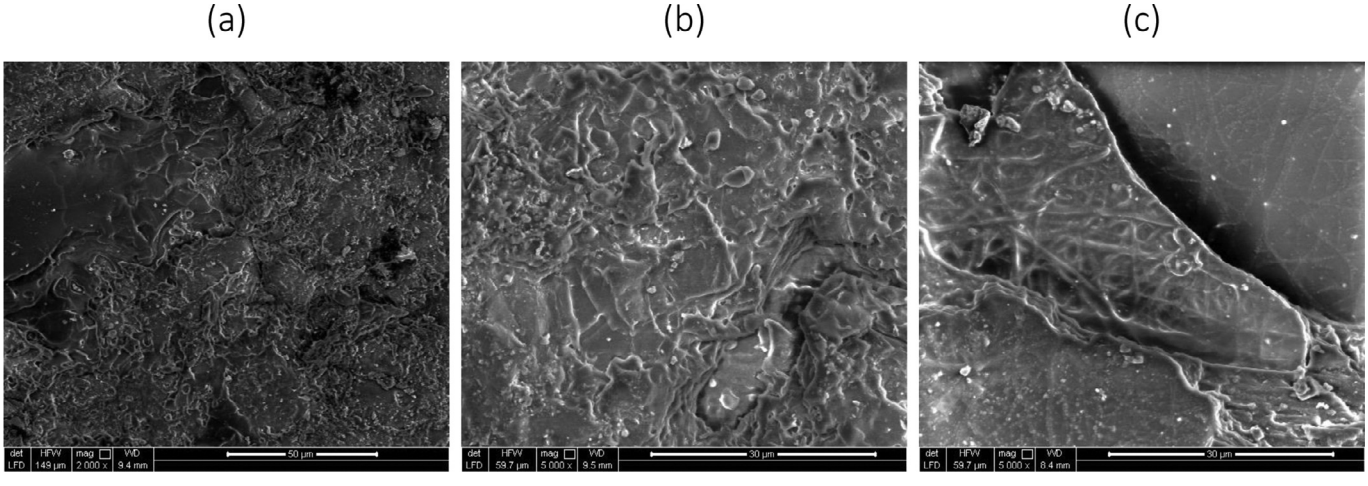

Fig. 15. SEM images of fracture surfaces of N 50 - 1 sample at different magnifications.

Conclusions

For the first time, rubbery electrospun NBR/PCL blend nanofibers were integrated into adhesive joints to evaluate their effect on the fracture toughness of high strength and high toughness 2k structural epoxy resin. Two curing cycles (70 °C for 5 h and 50 °C for 80 h) were performed to investigate the effect on possible resin toughening mechanisms.

By applying a curing cycle with temperatures below the melting temperature of the PCL crystalline fraction (55 ÷ 65 °C), the nanofibrous structure can be preserved. However, curing the adhesive at temperatures above the PCL melting is not sufficient to promote its complete mixing with the resin. Even if the nanofiber structure is not completely lost, the dispersion of the rubbery blend into the epoxy matrix should be improved. In this case, the nanomat acts as a vector for the toughening element.

Nano-reinforced joints exhibit the same fracture toughness value (G_{IC} = 0.63 N/mm for N 70 and G_{IC} = 0.58 N/mm for N 50) and similar failure mechanisms independently from the curing cycle used. This is also demonstrated by SEM images of nano-reinforced samples that reveal very similar fracture surfaces. However, the nanomat integration caused a fracture toughness reduction up to 45% if compared to virgin specimens cured at 70 °C.

Virgin specimens crosslinked at 50 °C revealed adhesion issues with the metal supports. The surface treatment could be not suitable for neat adhesive joints cured at 50 °C, as it does not allow cohesive fracture. As a result, low fracture toughness values are obtained (G_{IC} = 0.22 N/mm). From the DSC analyses, the cure at 70 °C seems to be slightly better, providing higher mechanical properties than the cure at 50 °C (as proved by 3PB tests) and probably better adhesion to the substrate. Indeed, at 70 °C the viscosity of the resin should be lower at the beginning of the curing cycle, so the wettability during cycle A should be improved with respect to cycle B.

The presence of rubbery nanomat, instead, allows the cohesive fractures also at 50 °C. It could prevent that the resin flows away, even if the viscosity profile during crosslinking was unfavourable. The nanomat prepreg favours the cracks propagation within the adhesive layer avoiding the unstable adhesive fractures that occur in virgin DCBs cured with non-standard cycle.

Declaration of Competing Interest

The authors declare that they have no known competing financial interests or personal relationships that could have appeared to influence the work reported in this paper.

Acknowledgements

The Authors wish to acknowledge the project “TEAM SAVE – E91B18000460007” (PG/2018/632196) of framework POR FESR 2014-2020 funded by Regione Emilia-Romagna with DGR 986/2018 for financial support.

References

Akpinar, I.A., Gürses, A., Akpinar, S., Gültekin, K., Akbulut, H., Ozel, A., 2018. Investigation of mechanical and thermal properties of nanostructure-doped bulk nanocomposite adhesives. J. Adhes. 94 (11), 847–866. doi:10.1080/00218464.2017.1415809.

Amada, S., Satoh, A., 2000. Fractal analysis of surfaces roughened by grit blasting. J. Adhes. Sci. Technol. 14 (1), 27–41. doi:10.1163/156856100742096, Jan..

Avci, A., Arikan, H., Akdemir, A., 2004. Fracture behavior of glass fiber reinforced polymer composite. Cem. Concr. Res. 34 (3), 429–434. doi:10.1016/j.cemconres.2003.08.027, Mar..

Bagheri, R., Marouf, B.T., Pearson, R.A., 2009. Rubber-toughened epoxies: a critical review. Polym. Rev. 49 (3), 201–225. doi:10.1080/15583720903048227, Aug..

Banea, M.D., da Silva, L.F.M., Carbas, R.J.C., Campilho, R.D.S.G., 2014. Mechanical and thermal characterization of a structural polyurethane adhesive modified with thermally expandable particles. Int. J. Adhes. Adhes. 54, 191–199. doi:10.1016/j.ijadhadh.2014.06.008, Oct..

Banea, M.D., Rosioara, M., Carbas, R.J.C., da Silva, L.F.M., 2018. Multi-material adhesive joints for automotive industry. Compos. Part B Eng. 151, 71–77. doi:10.1016/j.compositesb.2018.06.009, Oct..

Beckermann, G.W., Pickering, K.L., 2015. Mode I and Mode II interlaminar fracture toughness of composite laminates interleaved with electrospun nanofibre veils. Compos. Part Appl. Sci. Manuf. 72, 11–21. doi:10.1016/j.compositesa.2015.01.028, May.

Brugo, T., Musiari, F., Pirondi, A., Zucchelli, A., Cocchi, D., Menozzi, D., 2018. Development and fracture toughness characterization of a nylon nanomat epoxy adhesive reinforcement. Proc. Inst. Mech. Eng. Part J. Mater. Des. Appl. doi:10.1177/1464420718807733, 1464420718807730ct..

Burkholder, G.L., Kwon, Y.W., Pollak, R.D., 2011. Effect of carbon nanotube reinforcement on fracture strength of composite adhesive joints. J. Mater. Sci. 46 (10), 3370–3377. doi:10.1007/s10853-010-5225-6, May.

Caldona, E.B., De Leon, A.C.C., Pajarito, B.B., Advincula, R.C., 2017. A review on rubber-enhanced polymeric materials. Polym. Rev. 57 (2), 311–338. doi:10.1080/15583724.2016.1247102, Apr..

Cha, J., Kim, J., Ryu, S., Hong, S.H., 2019. Comparison to mechanical properties of epoxy nanocomposites reinforced by functionalized carbon nanotubes and graphene nanoplatelets. Compos. Part B Eng. 162, 283–288. doi:10.1016/j.compositesb.2018.11.011, Apr..

Cocchi, D., et al., 2020. Characterization of aluminum alloy-epoxy bonded joints with nanofibers obtained by electrospinning. J. Adhes. 96 (1–4), 384–401. doi:10.1080/00218464.2019.1666716, Mar..

da Silva, L.F.M., Öchsner, A., Adams, R.D. (Eds.), 2011. Handbook of Adhesion Technology. Springer, Heidelberg.

da Silva, Lucas.F.M., Carbas, R.J.C., Critchlow, G.W., Figueiredo, M.A.V., Brown, K., Sep. 2009. Effect of material, geometry, surface treatment and environment on the shear strength of single lap joints. Int. J. Adhes. Adhes. 29 (6), 621–632. doi:10.1016/j.ijadhadh.2009.02.012.

Daelemans, L., van der Heijden, S., De Baere, I., Rahier, H., Van Paepegem, W., De Clerck, K., 2016. Using aligned nanofibres for identifying the toughening micromechanisms in nanofibre interleaved laminates. Compos. Sci. Technol. 124, 17–26. doi:10.1016/j.compscitech.2015.11.021, Mar..

Daelemans, L., van der Heijden, S., De Baere, I., Rahier, H., Van Paepegem, W., De Clerck, K., 2017. Improved fatigue delamination behaviour of composite laminates with electrospun thermoplastic nanofibrous interleaves using the Central Cut-Ply method. Compos. Part Appl. Sci. Manuf. 94, 10–20. doi:10.1016/j.compositesa.2016.12.004, Mar..

Ebnesajjad, S., Ebnesajjad, C.F., 2014. Surface Treatment of Materials for Adhesive Bonding, second ed. William Andrew, an imprint of Elsevier, Amsterdam.

Ekrem, M., Avcı, A., 2018. Effects of polyvinyl alcohol nanofiber mats on the adhesion strength and fracture toughness of epoxy adhesive joints. Compos. Part B Eng. 138, 256–264. doi:10.1016/j.compositesb.2017.11.049, Apr..

Fernández, M.V., de Moura, M.F.S.F., da Silva, L.F.M., Marques, A.T., 2011. Composite bonded joints under mode I fatigue loading. Int. J. Adhes. Adhes. 31 (5), 280–285. doi:10.1016/j.ijadhadh.2010.10.003, Jul..

Fernando, D., Teng, J.G., Yu, T., Zhao, X.L., 2013. Preparation and characterization of steel surfaces for adhesive bonding. J. Compos. Constr. 17 (6), 04013012. doi:10.1061/(ASCE)CC.1943-5614.0000387, Dec..

Giuliese, G., Palazzetti, R., Moroni, F., Zucchelli, A., Pirondi, A., 2015. Cohesive zone modelling of delamination response of a composite laminate with interleaved nylon 6,6 nanofibres. Compos. Part B Eng. 78, 384–392. doi:10.1016/j.compositesb.2015.03.087, Sep..

Giv, A.N., Ayatollahi, M.R., Ghaffari, S.H., da Silva, L.F.M., Nov. 2018. Effect of reinforcements at different scales on mechanical properties of epoxy adhesives and adhesive joints: a review. J. Adhes. 94 (13), 1082–1121. doi:10.1080/00218464.2018.1452736.

Gude, M.R., Prolongo, S.G., Ureña, A., 2015. Toughening effect of carbon nanotubes and carbon nanofibres in epoxy adhesives for joining carbon fibre laminates. Int. J. Adhes. Adhes. 62, 139–145. doi:10.1016/j.ijadhadh.2015.07.011, Oct..

Gupta, S.K., Shukla, D.K., Ravindra, D.K., 2019. Effect of nanoalumina in epoxy adhesive on lap shear strength and fracture toughness of aluminium joints. J. Adhes. 0 (0), 1–23. doi:10.1080/00218464.2019.1641088, Jul..

Hamer, S., Leibovich, H., Intrater, R., Zussman, E., Siegmann, A., Sherman, D., 2011. Mode I interlaminar fracture toughness of nylon 66 nanofibrilmat interleaved carbon/epoxy laminates. Polym. Compos. 32, 1781–1789. doi:10.1002/pc.21210, Nov..

Han, X., Jin, Y., da Silva, L.F.M., Costa, M., Wu, C., 2020. On the effect of adhesive thickness on mode I fracture energy - an experimental and modelling study using a trapezoidal cohesive zone model. J. Adhes. 96 (5), 490–514. doi:10.1080/00218464.2019.1601087, Apr..

Huang, Z.-M., Zhang, Y.-Z., Kotaki, M., Ramakrishna, S., 2003. A review on polymer nanofibers by electrospinning and their applications in nanocomposites. Compos. Sci. Technol. 63 (15), 2223–2253. doi:10.1016/S0266-3538(03)00178-7, Nov..

Jakubinek, M.B., et al., 2015. Single-walled carbon nanotube–epoxy composites for structural and conductive aerospace adhesives. Compos. Part B Eng. 69, 87–93. doi:10.1016/j.compositesb.2014.09.022, Feb..

Jojibabu, P., Zhang, Y.X., Rider, A.N., Wang, J., Gangadhara Prusty, B., 2019. Synergetic effects of carbon nanotubes and triblock copolymer on the lap shear strength of epoxy adhesive joints. Compos. Part B Eng. 178, 107457. doi:10.1016/j.compositesb.2019.107457, Dec..

Khoramishad, H., Khakzad, M., 2018. Toughening epoxy adhesives with multi-walled carbon nanotubes. J. Adhes. 94 (1), 15–29. doi:10.1080/00218464.2016.1224184, Jan..

Kinloch, A.J., 1987. Adhesion and Adhesives. Springer Netherlands, Dordrecht.

Kinloch, A.J., 2003. Toughening epoxy adhesives to meet today’s challenges. MRS Bull. 28 (6), 445–448. doi:10.1557/mrs2003.126.

Kinloch, A.J., 2005. Adhesives in engineering. Proc. Inst. Mech. Eng. Part G J. Aerosp. Eng. doi:10.1243/0954410971532703.

Korayem, A.H., Chen, S.J., Zhang, Q.H., Li, C.Y., Zhao, X.L., Duan, W.H., 2016. Failure of CFRP-to-steel double strap joint bonded using carbon nanotubes modified epoxy adhesive at moderately elevated temperatures. Compos. Part B Eng. 94, 95–101. doi:10.1016/j.compositesb.2016.03.042, Jun..

Kozma, L., Olefjord, I., 1987. Surface treatment of steel for structural adhesive bonding. Mater. Sci. Technol. 3 (11), 954–962. doi:10.1179/mst.1987.3.11.954, Nov..

Krenk, S., 1992. Energy release rate of symmetric adhesive joints. Eng. Fract. Mech. 43 (4), 549–559. doi:10.1016/0013-7944(92)90198-N, Nov..

Leonard, L.W.H., Wong, K.J., Low, K.O., Yousif, B.F., 2009. Fracture behaviour of glass fibre-reinforced polyester composite. Proc. Inst. Mech. Eng. Part J. Mater. Des. Appl. 223 (2), 83–89. doi:10.1243/14644207JMDA224, Apr..

Maccaferri, E., Mazzocchetti, L., Benelli, T., Brugo, T.M., Zucchelli, A., Giorgini, L., 2020. Rubbery nanofibrous interleaves enhance fracture toughness and damping of CFRP laminates. Mater. Des. 195, 109049. doi:10.1016/j.matdes.2020.109049, Oct..

Maccaferri, E., Mazzocchetti, L., Benelli, T., Brugo, T.M., Zucchelli, A., Giorgini, L., 2020. Rubbery nanofibers by co-electrospinning of almost immiscible NBR and PCL blends. Mater. Des. 186, 108210. doi:10.1016/j.matdes.2019.108210, Jan..

Moroni, F., Palazzetti, R., Zucchelli, A., Pirondi, A., 2013. A numerical investigation on the interlaminar strength of nanomodified composite interfaces. Compos. Part B Eng. 55, 635–641. doi:10.1016/j.compositesb.2013.07.004, Dec..

Musiari, F., et al., 2018. Experimental investigation on the enhancement of Mode I fracture toughness of adhesive bonded joints by electrospun nanofibers. J. Adhes. 94 (11), 974–990. doi:10.1080/00218464.2017.1402301, Sep..

Oh, H.J., Kim, H.Y., Kim, S.S., 2014. Effect of the core/shell-structured meta-aramid/epoxy nanofiber on the mechanical and thermal properties in epoxy adhesive composites by electrospinning. J. Adhes. 90 (9), 787–801. doi:10.1080/00218464.2013.843458, Sep..

On, S.Y., Kim, M.S., Kim, S.S., 2017. Effects of post-treatment of meta-aramid nanofiber mats on the adhesion strength of epoxy adhesive joints. Compos. Struct. 159, 636–645. doi:10.1016/j.compstruct.2016.10.016, Jan..

Palazzetti, R., Zucchelli, A., 2017. Electrospun nanofibers as reinforcement for composite laminates materials – a review. Compos. Struct. 182, 711–727. doi:10.1016/j.compstruct.2017.09.021, Dec..

Palazzetti, R., Zucchelli, A., Trendafilova, I., 2013. The self-reinforcing effect of Nylon 6,6 nano-fibres on CFRP laminates subjected to low velocity impact. Compos. Struct. 106, 661–671. doi:10.1016/j.compstruct.2013.07.021, Dec..

Poorna Chander, K., Vashista, M., Sabiruddin, K., Paul, S., Bandyopadhyay, P.P., 2009. Effects of grit blasting on surface properties of steel substrates. Mater. Des. 30 (8), 2895–2902. doi:10.1016/j.matdes.2009.01.014, Sep..

Razavi, S.M.J., Neisiany, R.E., Ayatollahi, M.R., Ramakrishna, S., Khorasani, S.N., Berto, F., 2018. Fracture assessment of polyacrylonitrile nanofiber-reinforced epoxy adhesive. Theor. Appl. Fract. Mech. 97, 448–453. doi:10.1016/j.tafmec.2017.07.023, Oct..

C. K. Riew, A. R. Siebert, R. W. Smith, M. Fernando, and A. J. Kinloch, “Toughened epoxy resins: preformed particles as tougheners for adhesives and matrices,” in Toughened Plastics II, vol. 252, C.K. Riew and A.J. Kinloch, Eds. Washington, DC: American Chemical Society, 1996, pp. 33–44.

Saghafi, H., Palazzetti, R., Zucchelli, A., Minak, G., 2015. Influence of electrospun nanofibers on the interlaminar properties of unidirectional epoxy resin/glass fiber composite laminates. J. Reinf. Plast. Compos. doi:10.1177/0731684415584635, May.

Saraç, İ., Adin, H., Temiz, Ş., 2018. Experimental determination of the static and fatigue strength of the adhesive joints bonded by epoxy adhesive including different particles. Compos. Part B Eng. 155, 92–103. doi:10.1016/j.compositesb.2018.08.006, Dec..

Takeda, T., Narita, F., 2017. Fracture behavior and crack sensing capability of bonded carbon fiber composite joints with carbon nanotube-based polymer adhesive layer under Mode I loading. Compos. Sci. Technol. 146, 26–33. doi:10.1016/j.compscitech.2017.04.014, Jul..

Tsang, W.L., Taylor, A.C., 2019. Fracture and toughening mechanisms of silica- and core–shell rubber-toughened epoxy at ambient and low temperature. J. Mater. Sci. 54 (22), 13938–13958. doi:10.1007/s10853-019-03893-y, Nov..

van Dam, J.P.B., Abrahami, S.T., Yilmaz, A., Gonzalez-Garcia, Y., Terryn, H., Mol, J.M.C., 2020. Effect of surface roughness and chemistry on the adhesion and durability of a steel-epoxy adhesive interface. Int. J. Adhes. Adhes. 96, 102450. doi:10.1016/j.ijadhadh.2019.102450, Jan..

Wegman, R.F., 1989. Surface Preparation Techniques for Adhesive Bonding. Noyes Publications, Park Ridge, N.J., U.S.A.

Williams, R.J.J., Rozenberg, B.A., Pascault, J.-P., 1997. Reaction-induced phase separation in modified thermosetting polymers. In: Polymer Analysis Polymer Physics. Springer, Berlin, Heidelberg, pp. 95–156.

Wise, C.W., Cook, W.D., Goodwin, A.A., 2000. CTBN rubber phase precipitation in model epoxy resins. Polymer 41 (12), 4625–4633. doi:10.1016/S0032-3861(99)00686-2, Jun..

Yan, C.C., et al., 2020. The fracture performance of adhesively bonded orthodontic brackets: an experimental-FE modelling study. J. Adhes. 0 (0), 1–27. doi:10.1080/00218464.2020.1826320, Oct..

Zhang, H., Bharti, A., Li, Z., Du, S., Bilotti, E., Peijs, T., 2015. Localized toughening of carbon/epoxy laminates using dissolvable thermoplastic interleaves and electrospun fibres. Compos. Part Appl. Sci. Manuf. 79, 116–126. doi:10.1016/j.compositesa.2015.09.024, Dec..

Zielecki, W., Kubit, A., Trzepieciński, T., Narkiewicz, U., Czech, Z., 2017. Impact of multi-wall carbon nanotubes on the fatigue strength of adhesive joints. Int. J. Adhes. Adhes. 73, 16–21. doi:10.1016/j.ijadhadh.2016.11.005, Mar..

Zucchelli, A., Focarete, M.L., Gualandi, C., Ramakrishna, S., 2011. Electrospun nanofibers for enhancing structural performance of composite materials. Polym. Adv. Technol. 22 (3), 339–349. doi:10.1002/pat.1837.